The Bacteriorhodopsin Photocycle: Direct Structural Study of Two Substates of the M-Intermediate

Bong-Gyoon Han,*‡ Janet Vonck,‡§ and Robert M. Glaeser‡§

*Graduate Group in Biophysics, ‡Life Sciences Division, Donner Laboratory, Lawrence Berkeley Laboratory; and §Department of Molecular and Cell Biology, Stanley/Donner ASU, University of California, Berkeley, California 94720 USA

ABSTRACT Changes in protein structure that occur during the formation of the M photointermediate of bacteriorhodopsin can be directly visualized by electron diffraction techniques. A modified preparation technique for glucose-embedded crystals was employed to ensure sufficient hydration of the crystals, which was needed for the formation of the M intermediate at low temperature. Samples containing a high percentage of the M intermediate were trapped by rapidly cooling the crystals with liquid nitrogen after illumination with filtered green light at 240 and 260 K, respectively. Difference Fourier projection maps are presented for the M intermediates formed at these two temperatures. The diffraction data clearly show that statistically significant structural changes occur upon formation of the M intermediate at 240 K and then further upon formation of the second specimen that is produced at 260 K.

INTRODUCTION

Bacteriorhodopsin (bR) is a membrane protein from *Halobacterium halobium* that acts as a light-driven proton pump. This protein is a single polypeptide and contains a single prosthetic group, retinal. The structure of bR was solved by electron crystallography in the pioneering work of Henderson et al. (1990). Each bR monomer contains 7 transmembrane alpha helices, named A, B, C, D, E, F, and G from the N terminus to the C terminus (Fig. 1 *a*). The retinal is covalently linked to lysine 216 in the form of a protonated Schiff base. The Schiff base is located roughly in the middle of the protein, and it is believed to form an important "switch" midway within a proton channel (Mathies et al., 1991). The cytoplasmic half of the channel is narrow and hydrophobic, with the single exception of aspartate 96 as is described by Henderson et al. (1990). The extracellular half of the channel is wider and hydrophilic.

When light illuminates bR, protons are pumped from inside to outside, as part of the process in which the light-activated retinal drives a sequential photocycle. Intermediates of the photocycle can be distinguished by visible absorption spectroscopy. The intermediates are named bR, J, K, L, M, N, and O (Lozier and Niederberger, 1977; Mathies et al., 1991). The M-state intermediate is the only one in which the Schiff base is deprotonated, and as such it seems likely that structural changes between light-adapted bR and the M intermediate are particularly important in understanding the molecular mechanism of light-driven proton pumping.

An initial electron diffraction study (Glaeser et al., 1986) indicated that there was only a very small conformational change in the formation of the M intermediate. More recent neutron (Dencher et al., 1989) and x-ray (Koch et al., 1991; Nakasako et al., 1991) diffraction studies suggest that the structural change, although small, is bigger than first estimated. The most recent high resolution electron diffraction studies of frozen hydrated samples by Subramaniam et al. (1993) also show that there are significant conformational changes in the formation of the M intermediate. The discrepancy between the first electron diffraction work by Glaeser et al. and more recent diffraction studies can possibly be explained in terms of inadequate hydration of the glucose-embedded specimen. Fourier Transform Infra Red (FTIR) and visible spectroscopy work by Perkins et al. (1992) showed that hydration is a critical factor in allowing formation of the M intermediate when the sample is illuminated at low temperature.

Recently, the existence of at least two sequential M substates has been discussed (Varo and Lanyi, 1991a, b). By using FTIR spectroscopy, Ormos (1991) initially suggested that there exist two M substates called M_1 and M_2, which can be trapped at 240 and 260 K, respectively. However, additional blue-light photoreversal experiments by Ormos et al. (1992) have clearly attributed the differences in FTIR spectra, just described above, to differences in the amount of contaminating species, notably the N-intermediate. Ironically, the original spectroscopic differences reported by Ormos (1991) were confirmed by Perkins et al. (1992) with glucose-embedded samples, and in this case it was possible to rule out contamination by the N-intermediate as the basis for FTIR differences at 240 and 260 K. In the companion paper, using glucose-embedded samples, Vonck et al. (1994) show that a pure M-state is trapped at 240 K and that a mixture of the M-state, which is trapped at 240 K, and a different intermediate M_N (Sasaki et al., 1992) is trapped at 260 K, thereby reconciling the observation of Ormos et al. (1992) and Perkins et al. (1992).

Received for publication 3 February 1994 and in final form 3 June 1994.

Address reprint requests to Robert M. Glaeser, Life Sciences Division, Donner Lab., Lawrence Berkeley Laboratory, 1 Cyclotron Road, Berkeley, CA 94720. Tel.: 510-642-2905; 510-643-9290; E-mail: rmglaeser@lbl.bitnet.

Dr. Han's present address: Division of Biology, California Institute of Technology, Pasadena, CA 91125.

0006-3495/94/09/1179/08 $2.00

In this paper, we present high resolution difference Fourier maps, constructed using electron diffraction techniques. Using the conditions of the FTIR experiment of Perkins et al. (1992), different samples of M were trapped after illumination at 240 and 260 K to determine whether statistically significant differences in structure could be detected by means of the diffraction data. To overcome the difficulty in the formation of M-state intermediates at low temperature caused by partial dehydration, we have used a protocol like that of Perkins et al. (1992) for preparing humidified, glucose-embedded bR. The M-state samples prepared at the two temperatures both show significant structural changes from the resting (bR) state and from each other.

MATERIALS AND METHODS

bR crystals

Purple membrane was isolated and purified from *Halobacterium halobium* strain ET1001, according to the protocol of Oesterhelt and Stoeckenius (1971). For electron microscopy, the purified purple membranes were fused according to the protocol of Baldwin and Henderson (1984) to produce membrane patches with a diameter larger than 4 μm. Some trial and error is commonly required to get membrane sheets that are both large in diameter and not stacked together in the form of double-thickness crystals.

Sample preparation for diffraction experiments

Fused membranes were mixed with a glucose solution in pH 6.5, 10 mM MOPS buffer and loaded on a carbon film supported by a copper grid, as described by Glaeser and Downing (1990). The specimen grid with mixed solution was blotted with a filter paper in air that was equilibrated at 80% relative humidity by bubbling the air through a saturated ammonium sulfate solution. The grid was held in the flowing humid air for 10 min. Then the grid was rapidly plunged into liquid nitrogen in the dark.

The "frozen" specimen grid was transferred into a Gatan cryo-specimen holder under liquid nitrogen. The blade shutter of the specimen holder was opened to ambient air at a specimen temperature of 160 K for 90 s to condense an excess amount of ice on the specimen grid. This ice condensation step was needed to prevent dehydration of the sample in the stream of dry, cold nitrogen gas that was subsequently used for warming the sample to 240 or 260 K. After the ice condensation step, the blade shutter was closed and the specimen holder was inserted into a home made chamber in which the specimen temperature was equilibrated by flowing cold nitrogen gas at either 240 or 260 K. The automatic temperature control of the Gatan cryo-specimen holder was set to the corresponding temperature, and the temperature of the specimen holder was checked by reading both the Gatan temperature control gauge and another thermocouple placed in the flowing N_2 gas at a point near the specimen grid. When the temperature readouts of both the Gatan temperature control gauge and the thermocouple were stabilized at 240 or 260 K, as described, the blade shutter was opened to expose the specimen grid to previously focused, filtered green light for 30 s. Then liquid nitrogen was poured onto the grid and the green light was turned off. The two types of specimen produced in this way are referred to in the following text as M_{240K} and M_{260K}, respectively. After the temperature dropped below 210 K, the Gatan blade shutter was closed and the Gatan cryo-specimen holder was inserted into the electron microscope. The remaining excess amount of ice was sublimed by heating the sample to 180 K in the microscope vacuum for at least 15 min. Then the specimen grid was cooled again to 110 K in preparation for the diffraction data collection.

Two different sets of diffraction data were collected for the sample in the light adapted, bR568 state, to avoid any systematic error that could be caused by the two different maximum temperatures that are used as part of the sample preparation techniques for M_{240K} and M_{260K}. The bR568 data set needed for each substate was collected from samples that were prepared using the same protocol used to trap each M substate, but omitting the illumination by green light. These "reference" data sets are named bR_{240K} and bR_{260K}, respectively.

Electron diffraction

Electron diffraction data were recorded using a JEOL JEM 4000 EX electron microscope at an accelerating voltage of 400 kV. The beam diameter was adjusted to 3 μm on the specimen plane. The final accumulated electron dose was 3 electrons/Å^2. Electron diffraction patterns were digitized using a Perkin Elmer PDS densitometer with a step size of 10 μm. Background subtracted spot intensities were measured, and specimen tilt angles, tilt axes, temperature factors, scale factors, and twin proportions were refined using programs developed by Baldwin and Henderson (1984). Only those diffraction patterns were used that extended to at least 3.5 Å resolution, and that had minor twin proportions less than 10%. Unavoidable, small variations in tilt angle, within $\pm 5°$ resulted in a slight distribution of measured intensities along each reciprocal lattice line. Curves were fitted to the measured intensities for each reciprocal lattice line, and intensities at the (h, k, 0) plane were interpolated from the fitted curves. The final diffraction data were confined in the present study to 3.8-Å resolution. The final amplitude data in the (h, k, 0) plane were combined with the published phase data (Henderson et al., 1990) to produce difference Fourier projection maps. Contour levels for difference Fourier projection maps were chosen so that one contour level corresponds to one-tenth of the contour level used for the projection map in Fig. 1 *a*.

RESULTS

Effect of hydration

Sufficient hydration of glucose-embedded PM is essential for formation of the M-intermediate at low temperatures (Perkins et al., 1992; Perkins et al., 1993). To determine whether our hydration protocol itself would result in structural changes, we computed a difference Fourier map between PM equilibrated in 80% relative humidity and plunge-frozen, and PM prepared at ambient humidity in the conventional way, but then desiccated in vacuum at room temperature to reach a defined state. Hydrated samples were prepared for this preliminary work as described in Materials and Methods, but put into the electron microscope directly after freezing, avoiding the various other manipulations required to trap the M-intermediate states. Dehydrated samples were kept at ambient humidity for 30 min, inserted into the microscope, and kept in the microscope vacuum for 30 min before cooling. Diffraction patterns were recorded at 110 K in both cases.

A total of 12 films each were used to evaluate the differences between the hydrated and the dehydrated samples. Difference maps and controls based on these data are shown in Fig. 1. The difference map between hydrated and dehydrated samples, shown in Fig. 1 *b*, contains a large number of positive and negative peaks. To test the reproducibility of these features, two independent difference maps were calculated from separate halves of the data, i.e., 6 films for each set. These maps show essentially the same features, but with different variations in peak heights (not shown). The correlation coefficient for these two independent data sets is 0.69, showing that there is a significant difference in structure between the hydrated samples and the dry samples.

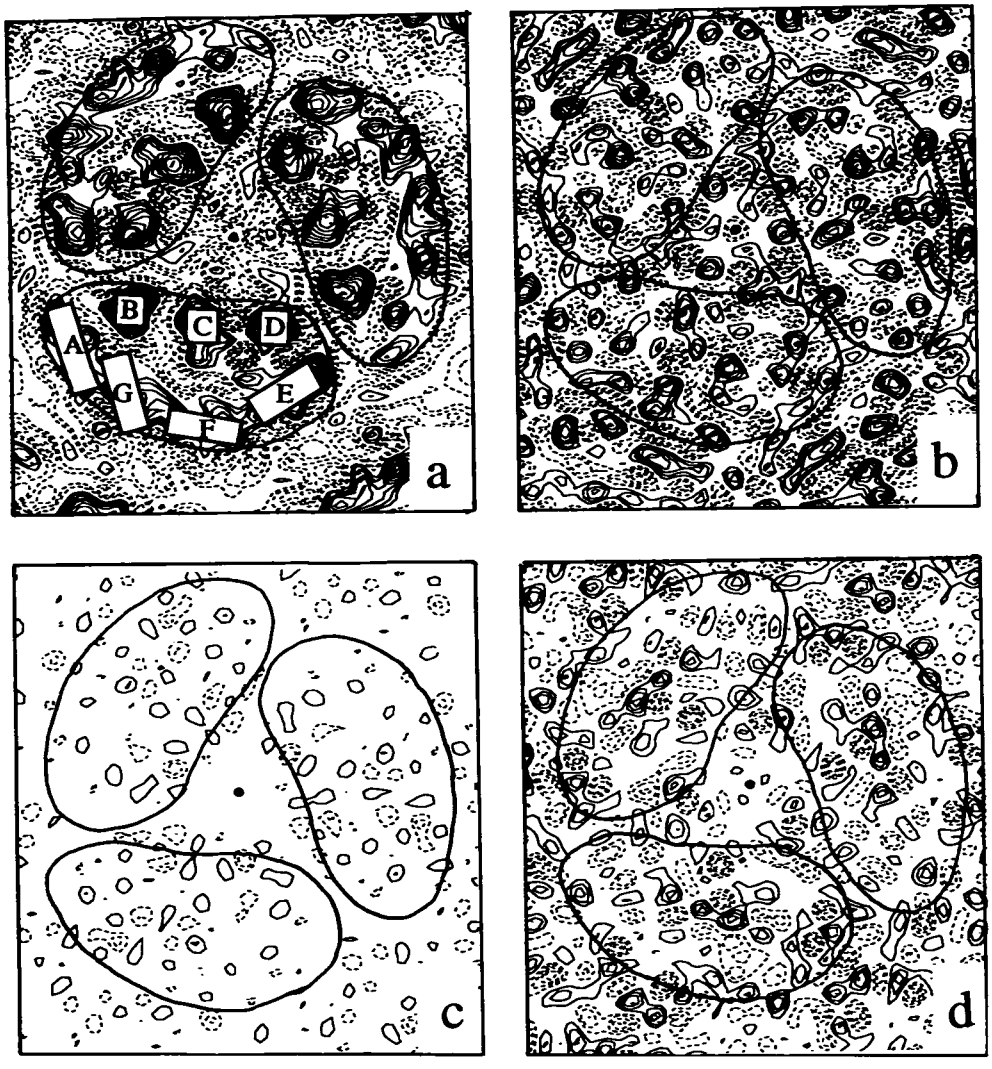

FIGURE 1 (*a*) Projection map of bR from the data of Henderson et al. (1990), shown here for reference, to identify the positions of difference peaks in subsequent maps. (*b–d*). Difference maps of glucose-embedded bR to show the effect of hydration. Continuous lines represent positive signals and discontinuous lines represent negative signals. Contour levels are one-tenth of those in *a*. The approximate protein boundary within the plane of the membrane is drawn. (*b*) Difference map for 12 films of bR equilibrated in 80% relative humidity minus 12 films of dry bR. (*c*) Difference map that shows the noise level in the data for humidified, glucose embedded bR. The 12 films in the "humidified specimen" data set were divided into two independent halves and processed as described in Materials and Methods, to give independent estimates of the (*h*, *k*, 0) intensities. (*d*) Difference map that shows the noise level in the data for dry bR.

The internal consistency of the hydrated data sets and the dehydrated data sets, respectively, was tested by dividing each set into two sets of 6 films and calculating the difference Fourier map between the halves. Features seen in these maps must result from random noise. An interesting outcome of this test is the finding that the noise level in the hydrated set (Fig. 1 *c*) is much lower than in the dehydrated data (Fig. 1 *d*). Evidently, the new preparation method, which maintains improved hydration, not only keeps the protein in a state that permits the photocycle to proceed to the M-state at low temperature (Perkins et al., 1992), but also ensures a more reproducible initial structure than is the case when using dry, glucose-embedded PM.

Difference amplitudes for the M substates prepared at the two different temperatures

The complete set of difference amplitudes along with the amplitudes for the M_{240K} and M_{260K} intermediates are shown in Table 1. A total of 12, 14, 14, and 12 films were used to construct the table for M_{240K}, bR_{240K}, M_{260K}, and bR_{260K}, respectively.

Difference Fourier maps for the M substates prepared at two different temperatures

The difference maps and controls for the M-intermediates are shown in Fig. 2. Fig. 2 *a* represents the difference map between the M_{240K} substate and the bR_{240K} reference data set. This map shows that small conformational changes occur throughout the molecular envelope of the protein monomer, and even within the area of the lipid, upon formation of the M intermediate. Major positive peaks with more than four contour levels appear near helices E and G. The highest peak is the one near helix G, with six contour levels. The most prominent negative peak appears directly over the position of the Schiff base. Fig. 2 *b* shows the difference noise map between two independent halves of the M_{240K} data set. Almost every peak in this noise map is within two contour levels. The height of peaks introduced by the formation of the M intermediate (Fig. 2 *a*) is obviously much higher than the height of peaks caused by noise alone (Fig. 2 *b*).

The difference map between the M_{260K} and the bR_{260K} reference data set is shown in Fig. 2 *c*. Major positive peaks that are higher than four contour levels appear near helices B, F, and G. The major negative peaks appear near helices F and

TABLE 1 Structure factor amplitudes and difference amplitudes

H	K	F_{M240K}	ΔF_{M240K}	F_{M260K}	ΔF_{M260K}	H	K	F_{M240K}	ΔF_{M240K}	F_{M260K}	ΔF_{M260K}
1	4	11431	−624	11439	−532	6	2	6071	219	5571	−287
1	5	16081	857	15590	286	6	3	2328	−336	2357	−411
1	6	3092	−280	2396	−1050	6	4	4790	−524	4989	−377
1	7	13189	−32	12479	−156	6	5	3156	−78	3240	172
1	8	4491	−529	4311	−84	6	6	1860	−586	2025	−349
1	9	5488	170	5353	379	6	7	4659	−432	4607	−57
1	10	3532	−522	3980	−335	6	8	9979	407	10039	516
1	11	4213	−111	3754	−626	6	9	1802	107	1627	−409
1	12	10706	1055	10206	367	6	10	3404	−191	3899	438
1	13	6955	−125	6707	−187	7	0	9220	267	9698	1030
2	3	7043	−463	7836	−2	7	1	10176	696	10158	780
2	4	20172	787	20031	−134	7	2	2546	−604	2468	−323
2	5	5309	−270	5805	151	7	3	4295	−994	4498	−619
2	6	7888	−43	7816	261	7	4	1739	−541	1570	−554
2	7	8380	−770	8425	−171	7	5	2858	−377	3684	534
2	8	9475	167	9861	782	7	6	2275	−1005	2858	−492
2	9	6540	604	6275	6	7	7	7771	1138	8028	813
2	10	4259	−619	4934	−205	7	8	1851	202	1347	−408
2	11	4952	−318	5323	−637	7	9	3662	−185	3492	−324
2	12	3977	−275	4189	−422	8	0	2754	−711	2747	−84
2	13	1678	−226	1538	−379	8	1	1871	−483	2136	−242
3	2	12827	825	13066	1068	8	2	5345	−588	5500	−601
3	3	2226	−170	3220	1225	8	3	4887	238	4981	637
3	4	14977	1012	14739	406	8	4	2922	−444	3318	18
3	5	13749	−764	14496	107	8	5	7369	617	7682	1056
3	6	3890	−704	4084	−305	8	6	4539	−617	4403	−909
3	7	6573	−331	6920	−10	8	7	3939	−402	3730	−377
3	8	4812	27	4706	586	8	8	5597	116	5383	161
3	9	3046	676	3328	829	9	0	4614	−47	4425	115
3	10	2558	254	2569	−100	9	1	7527	−862	8072	−441
3	11	7163	−104	6967	−74	9	2	4812	595	4228	85
3	12	4641	147	4737	130	9	3	5257	−262	5395	−151
4	0	12316	−128	12323	268	9	4	4732	109	5118	−79
4	1	15136	−94	14535	−749	9	5	5442	227	5391	−439
4	2	10774	−401	10867	−309	9	6	4028	−304	3658	−624
4	3	23590	−351	23737	−257	9	7	1660	−45	1487	−450
4	4	6353	556	6352	286	10	0	2566	−907	2428	−1523
4	5	4991	−630	5716	413	10	1	2418	273	2492	406
4	6	3611	−141	3426	188	10	2	5884	264	6361	381
4	7	5385	627	5464	851	10	3	8696	−546	8741	−288
4	8	5294	40	5893	777	10	4	1941	332	1564	−424
4	9	5181	428	4726	−319	10	5	6360	632	6451	806
4	10	6408	312	6640	250	10	6	2700	−65	2559	−117
4	11	2833	463	3044	911	11	0	5527	294	5711	443
5	0	17011	102	16897	−504	11	1	6225	993	5929	1241
5	1	4958	−131	4704	−157	11	2	4717	−903	5372	−83
5	2	17205	−142	16914	−663	11	3	4034	43	3648	−295
5	3	5136	−892	4902	−1048	11	4	1303	4	1160	−299
5	4	2518	−464	2730	46	11	5	5525	−116	5388	127
5	5	3204	143	2412	43	12	0	4457	−228	4928	67
5	6	3588	−161	3613	−305	12	1	1568	411	1094	−510
5	7	6044	−220	5763	−414	12	2	3143	338	3435	972
5	8	1526	−158	1580	−571	12	3	1581	−224	1615	−843
5	9	1579	32	1479	−377	13	0	3605	−747	4520	288
5	10	2121	−249	2328	−166	13	1	5465	−60	5318	−45
5	11	2415	−702	1746	−1216	13	2	6094	458	5970	402
6	0	12136	−10	12859	672	14	0	3156	1100	2604	349
6	1	14325	208	13970	−68						

G. Fig. 2 *d* represents the difference noise map between two independent M_{260K} data sets. Almost all peaks in this noise map are within two contour levels, which again are obviously much lower than the peak heights detected in the M_{260K} difference map.

Fig. 2 *e* shows the M_{260K} minus M_{240K} difference map calculated by subtracting Fig. 2 *a* from Fig. 2 *c*. A major positive peak with five contour levels appears between helices C and G, very close to the projected position of the Schiff base. Another positive peak with five contour levels appears between helices C and D. These two positive peaks appear to be coupled with nearby negative peaks.

The difference map between the bR_{260K} and bR_{240K} reference data sets is shown in Fig. 2 *f*. The peaks in this map represent both random errors in measurement plus potential systematic signals introduced by the different thermal history involved in the sample preparation techniques for these two reference data sets. The peak levels of the bR_{260K} minus bR_{240K} map shown in Fig. 2 *f* are slightly higher than those of the M_{240K} and M_{260K} noise maps shown in Fig. 2, *b* and *d*,

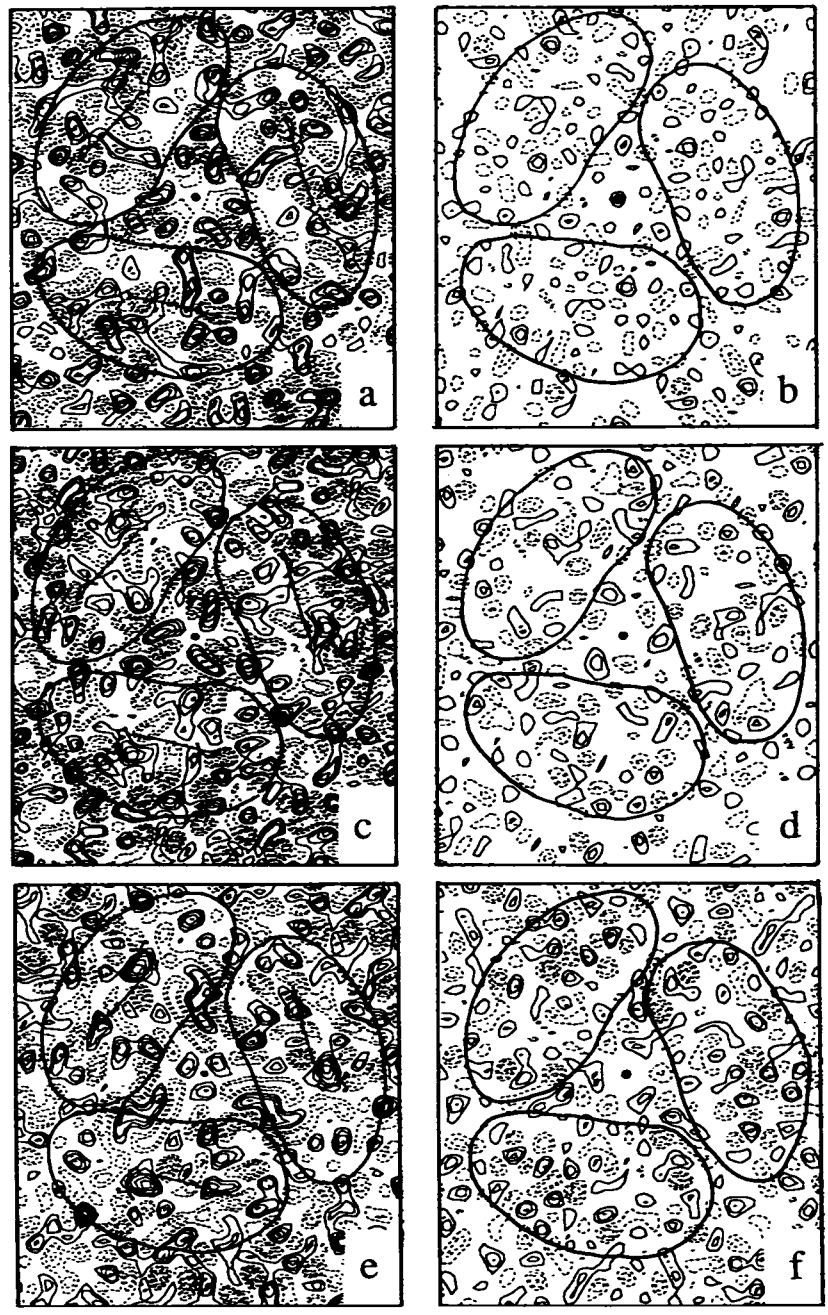

FIGURE 2 Difference Fourier projection maps for the M-intermediate at 3.8 Å resolution. All maps are contoured at one-tenth of the contour level used for the projection map shown in Fig. 1 *a*. Continuous lines represent positive signals and discontinuous lines negative signals. The approximate protein boundary of each monomer is drawn. (*a*) Difference map of structural changes that occur in the formation of M_{240K} at 240 K, obtained using 12 illuminated and 14 unilluminated crystals. The positions of lysine 216 and retinal are superimposed on the map. (*b*) Difference noise map between two independent M_{240K} data sets, each consisting of 6 films. (*c*) Difference map of structural changes that occur in the formation of M_{260K} at 260 K, obtained using 14 illuminated and 12 unilluminated crystals. The positions of lysine 216 and retinal are superimposed on the map. (*d*) Difference noise map between two independent M_{260K} data sets, each consisting of 7 films. (*e*) Difference map of structural changes that occur during the transition from the M_{240K} substate to the M_{260K} substate, obtained by subtracting *a* from *c*. (*f*) Difference map obtained by subtracting the bR_{240K} diffraction amplitudes from the bR_{260K} diffraction amplitudes.

both of which are formed from data collected from samples that had a single thermal history. This bR_{260K} minus bR_{240K} map suggests, therefore, that the different thermal cycling techniques used here to form the M_{240K} and M_{260K} substates can introduce a small amount of non-random signal. These data confirm that it is worthwhile to use appropriate reference samples (bR_{240K} and bR_{260K}, respectively) when calculating the M_{240K} and M_{260K} difference maps.

Statistical evaluation

To test the accuracy of the difference amplitude data, we divided each initial set of data into two data sets, and derived measurements of $F(h, k, 0)$ from each data set. $\Delta F(h, k, 0)$ data sets were constructed in two different ways for M_{240K} and M_{260K} data sets. In the first case, the measured M amplitude data were divided randomly into two halves, and two separate, independent $F(h, k, 0)$ values were derived from these two M amplitude data sets as described in Materials and Methods. All measured bR data, however, were used to produce a single $F(h, k, 0)$ data set. Two difference amplitude data sets were then constructed by subtracting the single bR, reference $F(h, k, 0)$ data set from the two independent M data sets.

In the other case, both the M and the bR data set were randomly divided into two halves, and two independent $F(h, k, 0)$ data sets were derived for bR as well as for M. Two independent difference amplitude data sets were then constructed by subtracting independent bR reference data sets from independent M data sets.

The similarity between independent data sets was evaluated by calculating the correlation coefficient (Hoel, 1971):

$$C = \frac{\Sigma \Delta F_1 \Delta F_2 - \frac{\Sigma \Delta F_1 \Sigma \Delta F_2}{n}}{\left\{\Sigma (\Delta F_1)^2 - \frac{(\Sigma \Delta F_1)^2}{n}\right\}^{1/2}\left\{\Sigma (\Delta F_2)^2 - \frac{(\Sigma \Delta F_2)^2}{n}\right\}^{1/2}},$$

where ΔF_1 and ΔF_2 are the difference amplitudes of the first and second data sets, and n is the total number of terms in the indicated summation. The calculated correlation coefficients for several different resolution zones are summarized in Tables 2 and 3 for the M_{240K} and M_{260K} data sets, respectively. The overall correlation coefficient of the M_{240K} data set for all reflections is slightly higher than that of M_{260K} (0.91 vs. 0.90) when single bR_{240K} and bR_{260K} reference data sets were used. The overall correlation coefficient of the M_{260K} data set, however, is higher than that of M_{240K} (0.79 vs. 0.68) when two independent reference data sets were used.

Table 4 represents the correlation coefficients between the ΔF values that we have measured for the two M samples, and previously published difference amplitude data sets for the M intermediate. The electron amplitude data from Subramaniam et al. (1993) were measured out to 3.5-Å resolution, and our data were limited to 3.8 Å, whereas the x-ray amplitude data from Nakasako et al. (1991) and Koch et al. (1991) were limited to 7 Å and involved the superposition of diffraction orders with identical (or unresolved) Bragg spacings. The difference amplitude data from Subramaniam et al. (1993) for the D96G mutant specimen are much more highly correlated with the M_{260K} than with the M_{240K} sample (0.81 vs. 0.43 for the low resolution zone (15.0–7.2 Å) and 0.69 vs. 0.34 for the full, 15.0–3.8 Å resolution zone). The ΔF values obtained by Subramaniam et al. (1993) for the wild-type M intermediate, however, are more highly correlated with M_{240K} than M_{260K} for the low resolution zone and equally correlated with M_{240K} and M_{260K} for the whole data. The x-ray difference amplitude data from Koch et al. (1991) are slightly better correlated with M_{240K} than with M_{260K}, whereas the x-ray difference amplitude data from Nakasako et al. (1991) are more highly correlated with the M_{260K} difference amplitude data than with the M_{240K} difference amplitude data.

TABLE 2 Statistical evaluation of the differences in diffraction amplitudes for bR_{240K} and M_{240K}

Resolution zone (Å)	Number of reflections	Correlation coefficients*	Correlation coefficients‡
15.0–7.2	26	0.89	0.84
7.2–5.3	28	0.95	0.76
5.3–4.4	30	0.89	0.74
4.4–3.8	31	0.88	0.40
All reflections	115	0.91	0.68

* The values of ΔF_1 are difference amplitudes between 6 M_{240K} and 14 bR_{240K} diffraction patterns. The values of ΔF_2 are difference amplitudes between another 6 M_{240K} and the same 14 bR_{240K} diffraction patterns.
‡ The values of ΔF_1 are difference amplitudes between 6 M_{240K} and 7 bR_{240K} diffraction patterns. The values of ΔF_2 are difference amplitudes between another 6 M_{240K} and another 7 bR_{240K} diffraction patterns.

TABLE 3 Statistical evaluation of the differences in diffraction amplitudes for bR_{260K} and M_{260K}

Resolution zone (Å)	Number of reflections	Correlation coefficients*	Correlation coefficients‡
15.0–7.2	26	0.91	0.88
7.2–5.3	28	0.88	0.69
5.3–4.4	30	0.93	0.82
4.4–3.8	31	0.89	0.72
All reflections	115	0.90	0.79

* The values of ΔF_1 are difference amplitudes between 7 M_{260K} and 12 bR_{260K} diffraction patterns. The values of ΔF_2 are difference amplitudes between another 7 M_{260K} and the same 12 bR_{260K} diffraction patterns.
‡ The values of ΔF_1 are difference amplitudes between 7 M_{260K} and 6 bR_{260K} diffraction patterns. The values of ΔF_2 are difference amplitudes between another 7 M_{260K} and another 6 bR_{260K} diffraction patterns.

As a reference, correlation coefficients for our M_{240K} and M_{260K} difference amplitude data sets were calculated. The correlation coefficient between the M_{240K} and M_{260K} data sets is 0.58 for the whole data, which is considerably lower than the correlation coefficients obtained for two halves of the M-bR data sets in Tables 2 and 3 (0.91 and 0.90 for M_{240K} and M_{260K}, respectively). The M_{260K} intermediate is more highly correlated with the D96G mutant specimen of Subramaniam et al. (1993) than with the M_{240K} intermediate (0.69 vs. 0.58).

DISCUSSION

The difference Fourier map between humidified and dehydrated samples (Fig. 1 *b*) shows that there are significant differences in structure between samples prepared by the usual type of "glucose embedding" technique and our new "hydration technique," which was developed to guarantee the normal formation of the M intermediate at low temperature (Perkins et al., 1993). In addition, we have found here that the noise level in humidified glucose-embedded samples is significantly lower than in the dry, glucose-embedded samples used by Glaeser et al. (1986). The rather high noise level in the data obtained from dry, glucose-embedded samples might have been an obstacle in detecting structural changes.

The large difference in projection maps of M minus bR at 240 and 260 K confirms that statistically significant conformational changes occur upon formation of the M-state intermediate at both temperatures and that there are real structural differences between the samples of M that are trapped at the two temperatures, as have been implied in the FTIR data (Perkins et al., 1992; Vonck et al., 1994). At both temperatures, only M is trapped, as shown by Perkins et al. (1992) using visible absorption spectroscopy. Exclusive formation of M under these conditions is further confirmed by the fact that blue light, which is only appreciably absorbed by the M_{412} intermediate, can drive the FTIR spectrum of such samples completely back to the bR ground state (Vonck et al., 1994). From this evidence, it can be concluded that there are at least two M-substates, each with a measurably different protein conformation.

TABLE 4 Correlation coefficients between the M substates and previously published difference amplitude data sets for the M intermediate

	$F_{M_{240K}} - F_{bR_{240K}}$		$F_{M_{260K}} - F_{bR_{260K}}$	
	Resolution zone			
	15.0–7.2Å	15.0–3.8Å	15.0–7.2Å	15.0–3.8Å
Subramaniam et al (1993)				
D96G mutant	0.43	0.34	0.81	0.69
Wild-type	0.60	0.52	0.39	0.52
Koch et al. (1991)	0.62		0.57	
Nakasako et al. (1991)	0.44		0.63	
$F_{M_{240K}} - F_{bR_{240K}}$	1.00	1.00	0.49	0.58

Using the FTIR and electron diffraction data, Vonck et al. (1994) showed that our M_{240K} samples are a pure M state and our M_{260K} samples can be a mixture of M_{240K}, which is a pure M substate, and M_N, which has the protein structure of N but the deprotonated Schiff base, which is a unique characteristic of M (Sasaki et al., 1992). Our partially dehydrated, glucose-embedded samples lack some mechanistically important water molecules, which are required for reprotonation of the Schiff base, once the protein has adopted the specific conformations of the N-state intermediate (Cao et al., 1991). The lack of water molecules needed for the reprotonation of the Schiff base, similar to the lack of the proton donor D96 in the D96N mutant, results in a substantial increase in the life time of the last M intermediate (M_N) (Váró and Lanyi, 1991c), otherwise too short lived to be detected.

Previous diffraction experiments and our current electron diffraction study agree that there are significant conformational changes that occur in the formation of the M intermediate, but there are some differences that have been seen in the positions and the relative heights of peaks. The differences between these diffraction studies now can be attributed, at least tentatively, to differences in sample preparation conditions. In the companion paper, Vonck et al. (1994) show that the relative proportion of different M substates can be significantly affected by several factors, such as hydration, temperature, and mutant versus wild-type. Also, the pH and the addition of arginine or guanidine can affect the relative proportion of M substates trapped. The amount of each M substate trapped, therefore, might have been quite different in the various maps published so far, because of different sample preparation conditions adopted by each group.

It is interesting that significant peaks are detected in the lipid region, where one might expect the difference map to show only noise peaks. The mutant difference map from Subramaniam et al. (1993) shows virtually identical peaks in the lipid region. One possible explanation for these peaks would be that the illumination used to induce the M state dehydrates the lipid and results in structural changes. This explanation is not likely to be true, because the factors that would affect dehydration were so different in the two sample preparation methods used by Subramaniam et al. and by ourselves. The different temperatures at which the M-state is formed is one significant factor that would affect dehydration differently in the two cases. In addition, our specimens were completely shielded by condensed ice to prevent dehydration during the period when the specimens were being illuminated. It seems likely, therefore, that movements within the protein during the formation of the M intermediate induce a real molecular shift in the lipid region, as well.

The high signal-to-noise ratio that we are now able to obtain in visualizing structural changes in the formation of the M substates indicates that it is justified to continue these electron diffraction measurements in three dimensions. M_{240K} specimens appear to contain a unique M-substate and are suitable for use in determining 3-D difference maps of this conformational intermediate. However, the fact that our M_{260K} sample is a mixture of two conformational states makes it less suitable for use in obtaining a 3-D difference map. The use of an appropriate mutant, such as the D96G mutant (Subramaniam et al., 1992), would seem to be a better way to get the 3-D difference map of the M_N intermediate. Recent progress in preparing flat bR specimens at liquid nitrogen temperature (Glaeser, 1992) have made it much easier to collect sharp diffraction patterns at the high tilt angles necessary for 3-D data collection, and this advance will facilitate the task of getting data that are accurate enough for use in calculating difference Fourier maps.

We thank K. H. Downing and R. Henderson for help in use of the MRC suite of programs. Also, we thank F. Burkard for help in building the special workstation needed for trapping M.

This work was supported by the Office of Health and Environmental Research, US Department of Energy (contract no. DE-AC03-76SF00098), and by a grant from the National Institutes of Health (GM 36884). J. Vonck was supported by a fellowship from the Netherlands Organization for Scientific Research (NWO). Use of the IVEM was supported by a grant from the National Institutes of Health (RR05097).

REFERENCES

Baldwin, J. M., and R. Henderson. 1984. Measurement and evaluation of electron diffraction patterns from two-dimensional crystals. *Ultramicroscopy.* 14:319–336.

Cao, Y., G. Váró, M. Chang, B. Ni, R. Needleman, and J. K. Lanyi. 1991. Water is required for proton transfer from Aspartate-96 to the bacteriorhodopsin Schiff base. *Biochemistry.* 30:10972–10979.

Dencher, N., G. Dresselhaus, G. Zaccai, and G. Büldt. 1989. Structural changes in bacteriorhodopsin during photon translocation revealed by neutron diffraction. *Proc. Natl. Acad. Sci. USA.* 86:7876–7879.

Glaeser, R. M. 1992. Specimen flatness of thin crystalline arrays: influence of the substrate. *Ultramicroscopy.* 46:33–43.

Glaeser, R. M., J. M. Baldwin, T. A. Ceska, and R. Henderson. 1986. Electron diffraction analysis of the M412 intermediate of bacteriorhodopsin. *Biophys. J.* 50:913–920.

Glaeser, R. M., and K. H. Downing. 1990. The "specimen flatness" problem in high-resolution electron crystallography of biological macromolecules. *Proc. XII Int. Congr. Elect. Microsc.* 1:98–99.

Henderson, R., J. M. Baldwin, T. A. Ceska, F. Zemlin, E. Beckmann, and K. H. Downing. 1990. Model for the structure of bacteriorhodopsin based on high-resolution electron cryo-microscopy. *J. Mol. Biol.* 213:899–929.

Hoel, P. G. 1971. Introduction to Mathematical Statistics. Fourth Ed. John Wiley & Sons, New York. 164.

Koch, M. H. J., N. A. Dencher, D. Oesterhelt, H.-J. Plöhn, G. Rapp, and G. Büldt. 1991. Time-resolved X-ray diffraction study of structural changes associated with the photocycle of bacteriorhodopsin. *EMBO J.* 10:521–526.

Lozier, H. L., and W. Niederberger. 1977. The photochemical cycle of bacteriorhodopsin. *Fed. Proc.* 36:1805–1809.

Mathies, R. A., S. W. Lin, J. B. Ames, and W. T. Pollard. 1991. From femtoseconds to biology: mechanisms of bacteriorhodopsin's light-driven proton pump. *Annu. Rev. Biophys. Chem.* 20:491–518.

Nakasako, M., M. Kataoka, Y. Amemiya, and F. Tokunaga. 1991. Crystallographic characterization by X-ray diffraction of the M-intermediate from the photo-cycle of bacteriorhodopsin at room temperature. *FEBS Lett.* 292:73–75.

Oesterhelt, D., and W. Stoeckenius. 1971. Rhodopsin-like protein from the purple membrane of *Halobacterium halobium*. *Nature New Biol.* 233: 149–152.

Ormos, P. 1991. Infrared spectroscopic demonstration of a conformational change in bacteriorhodopsin involved in proton pumping. *Proc. Natl. Acad. Sci. USA.* 88:473–477.

Ormos, P., K. Chu, and J. Mourant. 1992. Infrared study of the L, M, and N intermediates of bacteriorhodopsin using the photoreaction of M. *Biochemistry.* 31:6933–6937.

Perkins, G. A., F. Burkard, E. Liu, and R. M. Glaeser. 1993. Glucose alone does not completely hydrate bacteriorhodopsin in glucose-embedded purple membrane. *J. Microsc.* 169:61–65.

Perkins, G. A., E. Liu, F. Burkard, E. A. Berry, and R. M. Glaeser. 1992. Characterization of the conformational change in the M_1 and M_2 substates of bacteriorhodopsin by the combined use of visible and infrared spectroscopy. *J. Struct. Biol.* 109:142–151.

Sasaki, J., Y. Shichida, J. K. Lanyi, and A. Maeda. 1992. Protein changes associated with reprotonation of the Schiff base in the photocycle of Asp^{96}→Asn bacteriorhodopsin. *J. Biol. Chem.* 267:20782–20786.

Subramaniam, S., M. Gerstein, D. Oesterhelt, and R. Henderson. 1993. Electron diffraction analysis of structural changes in the photocycle of bacteriorhodopsin. *EMBO J.* 12:1–8.

Váró, G., and J. K. Lanyi. 1991a. Kinetic and spectroscopic evidence for an irreversible step between deprotonation and reprotonation of the Schiff base in the bacteriorhodopsin photocycle. *Biochemistry.* 30:5008–5015.

Váró, G., and J. K. Lanyi. 1991b. Thermodynamic and energy coupling in the bacteriorhodopsin photocycle. *Biochemistry.* 30:5016–5022.

Váró, G., and J. K. Lanyi. 1991c. Distortions in the photocycle of bacteriorhodopsin at moderate dehydration. *Biophys. J.* 59:313–322.

Vonck, J., B.-G. Han, F. Burkard, G. A. Perkins, and R. M. Glaeser. 1994. Two progressive substates of the M-intermediate can be identified in glucose-embedded, wild-type bacteriorhodopsin. *Biophys. J.* 67: 1173–1178.